Precious opal formation in Australia: Insights into Martian weathering processes

Gemma Emily Roberts

Abstract

Minerals reported in the Great Artesian Basin in central Australia have also been reported on the surface of Mars. The drying out of central Australia, during which time the peak production of opals occurred, is analogous to the drying out of the Martian surface *ca.* 3.7 Ga. This study documents, for the first time, minerals preserved in opal veins as interpreted from VNIR-SWIR and Raman spectroscopy. Minerals detected include Al-rich phyllosilicates (kaolinite/halloysite, montmorillonite), iron oxides and oxyhydroxides (hematite, goethite, maghemite, ferrihydrite, and possibly schwertmannite), and sulfates (gypsum, alunite, and possibly barite and jarosite). Trace elemental abundances across opal veins were also documented via LA-ICP-MS to examine materials that were unable to be determined by VNIR-SWIR or Raman spectroscopy. This study suggests that mineral assemblages trapped in opaline silica may provide clues to ancient and acidic environments on Mars.

1. Introduction

The bulk of the world's precious opal has its origin in a deeply weathered profile in the Great Artesian Basin (GAB) of central Australia. The large volume of amorphous silica in this profile, and the low temperature environment at which it formed, suggests acidic weathering at the scale of the GAB (e.g. Rey, 2013). Low pH weathering on a regional scale is unusual on Earth, due to the abundance of carbonates. Remarkably, the GAB contains little carbonate, as it formed in the cold, muddy, anoxic and shallow Eromanga continental sea that flooded central Australia from 125-95 Myr ago. Regression followed mid-Cretaceous flooding, and the prevailing oxidising conditions caused the release of sulphuric acid from biogenic pyrite; this resulted in a long period of weathering in an acidic environment. Rey (2013) deduced that the peak production of precious opal occurred between 95 and 60 Ma, during uplift and erosion of the GAB, after which time the landscape was stable. For the past 60 Myr, early weathering minerals have been constantly reworked through continuous weathering (Taylor and Shirtliff, 2003), however, inclusions in precious opals have preserved minerals characteristic of acidic weathering.

Minerals that have been reported in the weathered profile at the surface of the GAB include opaline silica, phyllosilicates (kaolins and smectite), sulfates (jarosite, alunite and gypsum) and iron oxides (goethite and hematite) (e.g. Exon and Senior, 1976; Senior, 1979; Simon-Coinçon *et al*., 1996; Roberts *et al*., 2014). Interestingly enough, spectral signatures of the surface of Mars indicate a variety of hydrated minerals, including opaline silica, phyllosilicates, sulfates, and iron oxides, with their formation attributed to a long-lived low-temperature aqueous weathering history (e.g. Ehlmann *et al*., 2013) followed by a period of intense acidic oxidative weathering (e.g. Carter *et al*., 2013). The mineral assemblages shared by both the

GAB and Mars suggest that inclusions in precious opals offer a unique access to Martian weathering processes.

The objective of this project is to document the mineralogical assemblages preserved in inclusions in precious opal veins using Visible Near-Infrared to Short-Wave Infrared (VNIR-SWIR) spectroscopy, Raman spectroscopy, and Laser-Ablation Inductively-Coupled-Plasma Mass Spectrometry (LA-ICP-MS).

2. Materials and Methods

VNIR-SWIR spectroscopy is currently used to survey the surface of Mars, while a Raman spectrometer will be included in the suite of instruments on the European Space Agency's 2018 ExoMars rover. These techniques, therefore, offer a direct point of comparison with the GAB. LA-ICP-MS was used to identify the concentration and distributions of elements within different zones across opal veins.

Six key opal samples derived from early Cretaceous sediments were selected from the mining localities of Yowah (3 samples), Quilpie (2 sample), and Coober Pedy (1 sample), shown in Fig. 1. All samples contain opal found in veins or fractures and are considered typical of the mining area in terms of host rock composition. Rock samples were cut to expose cross sections of the opal veins, but no polishing was undertaken on hand samples. The thin section from Coober Pedy was polished. The thickness of the opal veins studied are ≤1 mm, and the thin section is ~120 μm thick. Photographs of the samples studied are shown in Fig. 2. Table 1 summarises the techniques undertaken on samples.

Table 1. *Details of opal samples with analytical techniques.*

Sample name	Locality	Host rock formation	Sample type	Analyses		
				VNIR-SWIR	Raman spectroscopy	LA-ICP-MS
Y-1	Yowah	Winton Formation	Hand sample	X	X	
Y-2	Yowah	Winton Formation	Hand sample	X	X	X
Y-3	Yowah	Winton Formation	Hand sample	X	X	X
Q-1	Quilpie	Winton Formation	Hand sample	X	X	X
Q-2	Quilpie	Winton Formation	Hand sample			X
CP-1	Coober Pedy	Bulldog Shale	Thin section		X	

2.1 VNIR – SWIR

VNIR – SWIR analyses were conducted on hand samples Y-1, Y-2, Y-3, and Q-1. Measurements were carried out with two line scanner sensors (made by Specim of Finland), a VNIR (spectral range 400 – 970

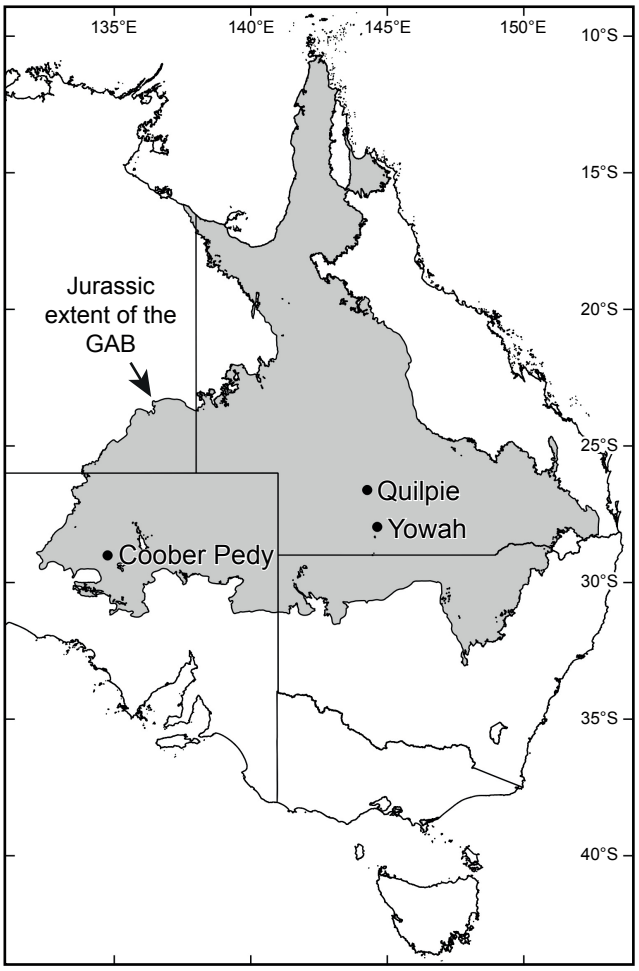

Figure 1. *Location of mining towns from which opal samples originate.*

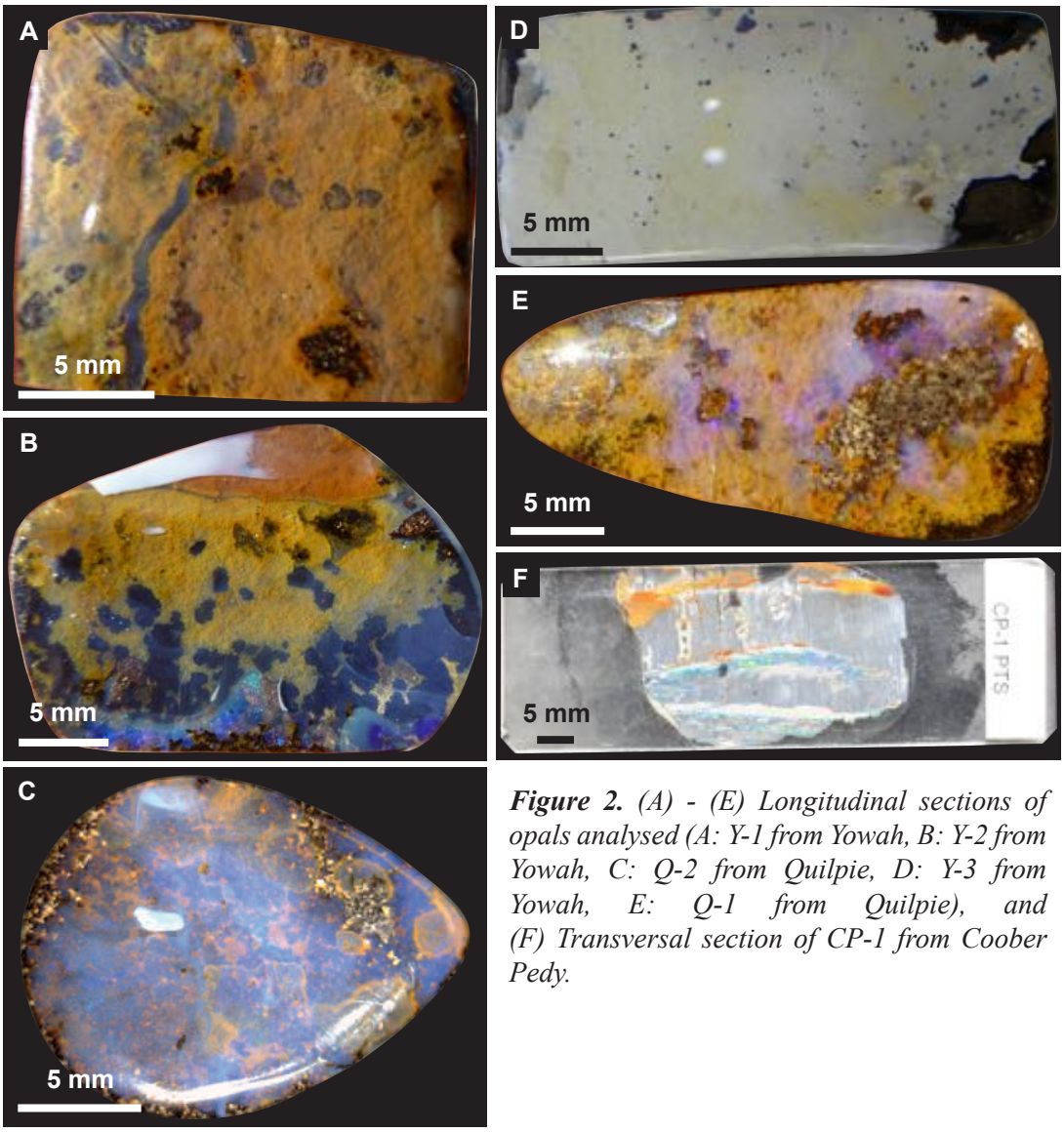

Figure 2. *(A) - (E) Longitudinal sections of opals analysed (A: Y-1 from Yowah, B: Y-2 from Yowah, C: Q-2 from Quilpie, D: Y-3 from Yowah, E: Q-1 from Quilpie), and (F) Transversal section of CP-1 from Coober Pedy.*

nm) and a SWIR (spectral range 970 – 2500 nm), at the Rio Tinto Centre for Mine Automation at the University of Sydney. The VNIR sensor recorded 125 band at an average full-width at half-maximum (FWHM) of 4.63 nm, and the SWIR sensor recorded 246 bands at an average FWHM of 6.23 nm. A spatial resolution of 0.304 mm^2 per pixel was achieved. Calibration measurements were acquired separately for each sensor by placing a calibration panel at one end of the scanning table.

2.2 Raman spectroscopy

Raman spectroscopic analyses were conducted on hand samples Y-1, Y-2, Y-3, Q-1, and thin section CP-1. No effort was made to optimise the Raman signal by adjusting the orientation of the minerals. Measurements were carried out at the Vibrational Spectroscopy Core Facility at the University of Sydney with a Renishaw InVia Raman microscope equipped with a ModuLaser plasma tube laser operating at 514 nm and 633 nm, and a 2400 lines/mm grating and 1200 lines/mm, respectively. The microscope was focused onto the sample using a 20× objective lens. The instrument was operated in the line focus confocal mode with detector exposure times between 10 and 60 seconds, and 1 to 20 spectra accumulations. Backscattered Raman signals were collected with a standard CCD detector using a maximum laser power of 3.87 mW at the sample. Calibration was verified with the ~520 cm^{-1} band of a polished silicon wafer.

2.3 LA-ICP-MS

LA-ICP-MS analyses were carried out on hand samples Y-2, Y-3, Q-1, and Q-2. Ablation was performed using the Gübelin Gem Lab's NWR193uc ESI laser with a PerkinElmer ELAN DRC-e quadruple ICP-MS in Lucerne, Switzerland. One hundred spots of 60 μm diameter each were analysed, comprised of 51 detectable major and trace elements. The energy beam used was ~4.5 J/cm^2 and the laser pulse frequency 5 Hz on opal and 10 Hz on brown material. The primer reference material used was NIST 610, and silica was used as an internal standard. Ablation of the sample was for 30 seconds, following a 40 second blank. The limits of detection vary for all elements, and where the reading was below the limit of detection the value was noted as '<LOD'.

3. Results

3.1 VNIR-SWIR distribution of minerals in opal veins and host rock

The four opal samples studied shared common minerals including phyllosilicates and iron oxides/oxyhydroxides. The spectra all have features that indicate the presence of at least two minerals, however this may be due to the spatial resolution being larger than a particular grain or crystal rather than a mineral mixture.

3.1.1 VNIR detector spectral results

Absorption features in the visible to near-infrared (VNIR) spectral range (0.40 – 1.0 μm) are due to ferrous iron (Fe^{2+}) and ferric iron (Fe^{3+}) electronic processes (Hunt, 1977). The spectral signatures of these iron oxides dominate the spectral features in the VNIR region, even when mixed with or coating clay minerals (Parente *et al*., 2008). The ferric minerals show a band maximum from 0.73 – 0.82 μm, and a band minimum from 0.85 – 0.98 μm (Sherman *et al*., 1982; Morris *et al*., 1985; Bishop *et al*., 1995; Bishop and Murad, 1996). Goethite, hematite, and lepidocrocite also show a Fe^{3+} absorption feature near 0.67 μm (Bishop and Murad, 1996; Murphy *et al*., 2014). The positions of these features indicate which mineral is present. Al-rich phyllosilicates do not have features in the VNIR, however, substitution of minor iron in place of aluminium may result in a weak shoulder at ~0.50 μm (McKeown *et al*., 2009). Spectra at ~0.90 μm are extremely noisy due to a fall-off in VNIR sensor sensitivity and atmospheric absorption by water (Murphy *et al*., 2013), therefore mineral identification was based on the position of the band maximum at ~0.75 μm and comparison with USGS laboratory spectra.

3.1.2 SWIR detector spectral results

Absorption features in the short-wave infrared (SWIR) spectral region (1.0 – 2.5 μm) are due to combinations and overtones of vibrational processes of molecules (Hunt, 1977). Absorptions near 1.4 μm are due to combinations and overtones of water (H_2O) and hydroxyl (OH) stretching molecules in the mineral structure (Hunt, 1977). Absorptions near 1.9 μm are due to combinations of H_2O stretching and bending overtones (McKeown *et al*., 2009). The absence of this band indicates the lack of water in a minerals structure (Clark *et al*., 1990). Absorptions in the region around 2.2 – 2.3 μm are due to OH stretching and bending (Clark *et al*., 1990). Absorptions near 2.2 μm are due to Al-OH or Si-OH stretching and bending combinations (McKeown *et al*., 2009). The identification of minerals with absorptions at the same wavelength is determined by differences in band shape and depth (McKeown *et al*., 2009). Mineral identification in the SWIR region was based on band position, shape and depth, with comparison with USGS laboratory spectra and published literature.

3.1.3 Iron oxides and oxyhydroxides

Five types of iron oxides and oxyhydroxides were identified in samples: hematite, goethite, maghemite, ferrihydrite, and possibly schwertmannite. Distinguishing features include a peak near 0.75 μm and the shape of the spectra in the VNIR. Band maxima for these ferric minerals are: 0.73 μm for akaganéite, 0.73 – 0.74 μm for schwertmannite, ~0.74 – 0.76 μm for hematite, ~0.76 – 0.765 μm for goethite, ~0.78 μm for maghemite, ~0.79 – 0.82 μm for lepidocrocite, and ~0.80 μm for ferrihydrite, (Morris *et al*., 1985; Bishop *et al*., 1993; Bishop and Murad, 1996).

The spectrum in Fig. 3A, from the vein wall, shows a peak at 0.78 that is consistent with maghemite. The shape of the spectrum in the VNIR could also indicate the presence of goethite. The spectra in Fig. 3B, 3D and 3E, have a band maximum at 0.75 μm, clearly consistent with goethite. The spectrum in Fig. 3G shows features in the VNIR consistent with goethite (band maximum at 0.77 μm), but features in the SWIR consistent with ferrihydrite or lepidocrocite (broad absorptions near 1.42 μm and 1.92 μm). The spectra in Fig. 3C and 3F show two peaks in the VNIR, where the second at 0.75 μm is consistent with hematite. The spectra in Fig. 3H show two peaks in the VNIR, where the second one at 0.733 μm is consistent with schwertmannite or akaganéite. The SWIR in Fig. 3H shows a broad absorption from 1.90 – 1.96 μm and is consistent with ferrihydrite, schwertmannite, or lepidocrocite, combined with opal, but not akaganéite (Bishop *et al*., 2015).

3.1.4 Phyllosilicates

Two types of phyllosilicates were identified along the vein walls and in the veins themselves: kaolin group minerals (kaolinite/halloysite) and montmorillonite. These Al-rich clays exhibit absorption features around 2.2 μm, due to Al-OH overtones, which vary in shape depending on the mineral present. Kaolinite exhibits a OH absorption at 1.41 μm and an asymmetric Al-OH doublet at 2.16 μm and 2.21 μm (e.g. Clark *et al.*, 1990). Halloysite exhibits a strong H_2O absorption at 1.91 μm, in addition to the same absorption features as kaolinite (e.g. McKeown *et al*., 2009). Montmorillonite has an OH absorption with an H_2O shoulder at 1.41 μm and 1.46 μm, respectively, a strong H_2O feature at 1.92 μm, and a sharp Al-OH absorption at 2.21 μm (e.g. Clark *et al*., 1990; McKeown *et al*., 2009).

In the spectra in Fig. 3A, 3B, and 3E a small doublet indicative of kaolinite/halloysite is present at 1.39 μm to 1.41 μm, but is much shallower than laboratory spectra. The spectrum in Fig. 3E has a shoulder at 1.45 μm which may indicate the presence of montmorillonite. The deep H_2O band at 1.91 μm is consistent with halloysite and montmorillonite, whereas the doublet at 2.16 μm and 2.21 μm is consistent with both kaolinite and halloysite. These features are consistent with spectra of laboratory mixtures consisting of kaolinite and montmorillonite. A comparison of this spectrum with published data suggests a mix of 50% kaolinite and 50% montmorillonite up to 75% kaolinite and 25% montmorillonite (McKeown *et al*., 2011; Cuadros and Michalski, 2013). At less than 50% kaolinite the doublet near 1.41 μm is lost, and with decreasing amount the shoulder at 1.45 μm becomes more prominent, while the doublet at 2.16 μm decreases in depth (McKeown *et al*., 2011; Cuadros and Michalski, 2013). Therefore, it seems likely that the spectra are mixtures of kaolinite with montmorillonite.

The spectrum in Fig. 3F shows features indicative of montmorillonite, including a 1.41 μm band with a slight shoulder at 1.45 μm, a deeper absorption at 1.91 μm, and a weak 2.21 μm band. The montmorillonite spectra observed have a weaker 2.21 μm hydration band than laboratory spectra indicating that it may be mixed with another mineral, such as goethite.

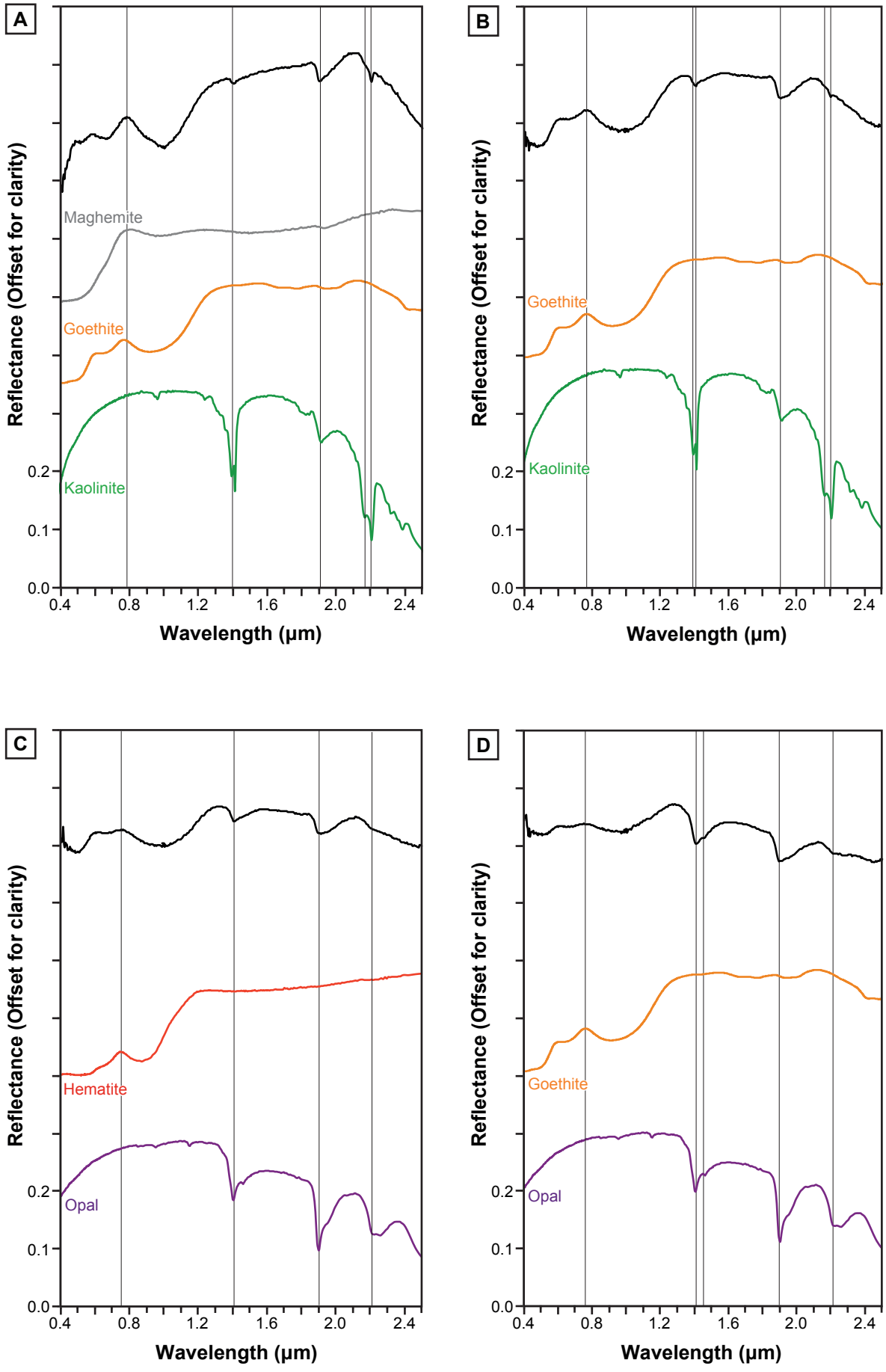

Figure 3 (continued over page)

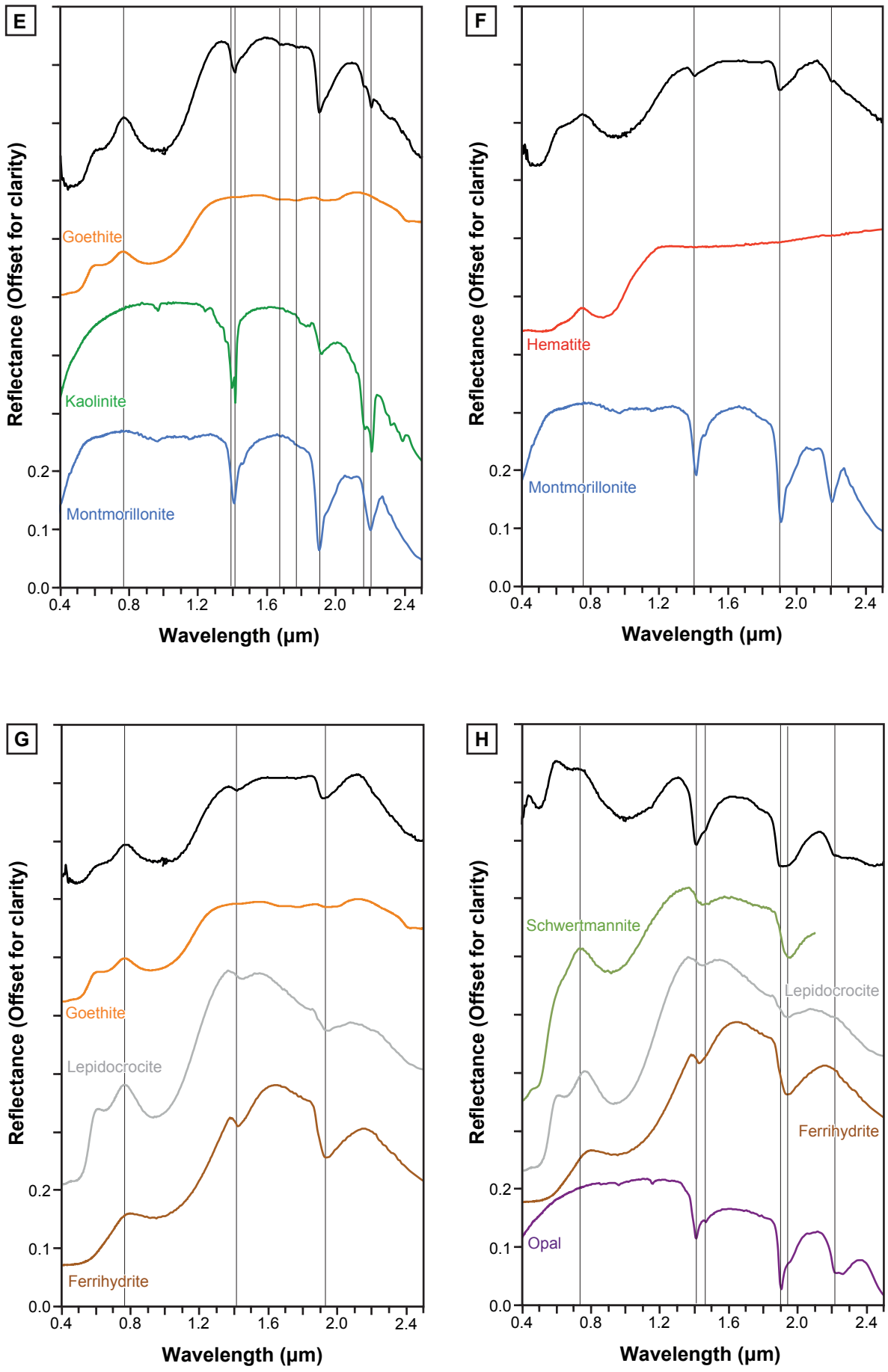
E
Reflectance (Offset for clarity)
Goethite
Kaolinite
Montmorillonite
0.0
0.1
0.2
0.4
0.8
1.2
1.6
2.0
2.4
Wavelength (μm)
F
Reflectance (Offset for clarity)
Hematite
Montmorillonite
0.0
0.1
0.2
0.4
0.8
1.2
1.6
2.0
2.4
Wavelength (μm)
G
Reflectance (Offset for clarity)
Goethite
Lepidocrocite
Ferrihydrite
0.0
0.1
0.2
0.4
0.8
1.2
1.6
2.0
2.4
Wavelength (μm)
H
Reflectance (Offset for clarity)
Schwertmannite
Lepidocrocite
Ferrihydrite
Opal
0.0
0.1
0.2
0.4
0.8
1.2
1.6
2.0
2.4
Wavelength (μm)

Figure 3

Figure 3. *VNIR-SWIR spectra of the variations of minerals detected in Y-1, Y-2, Y-3, and Q-1. The top black spectrum in each plot was from the samples in this study, and the coloured lines shown below are USGS laboratory spectra of identified minerals. (A) Maghemite, goethite, and kaolinite in vein wall in Y-3. (B) Goethite and kaolinite in vein wall in Y-1. (C) Hematite in opal in Y-1. (D) Goethite in opal in Q-1. (E) Goethite, kaolinite/halloysite, and montmorillonite in Q-1. (F) Hematite and montmorillonite in Y-1. (G) Goethite, lepidocrocite, or ferrihydrite in Y-1. (H). Ferrihydrite, schwertmannite, or lepidocrocite in opal in Y-1.*

3.2 Raman spectra of minerals

Minerals identified via Raman spectroscopy include goethite, hematite, gypsum, alunite, and possibly the sulfates jarosite and barite. Mineral identification was based on comparison with published literature.

3.2.1 Iron oxides and oxyhydroxides

Goethite was detected in Y-1, Y-2, Q-1, and CP-1. The Raman spectrum for each sample differed slightly (Fig. 4A), with bands at ~243 cm^{-1} (weak), ~300 cm^{-1} (strong), ~396 cm^{-1} (very strong), ~479 cm^{-1} (very weak), ~555 cm^{-1} (strong), ~684 cm^{-1} (strong), and ~996 cm^{-1} (weak). These values correspond with previously published values where bands were noted at ~243 cm^{-1}, ~298 cm^{-1}, ~385 cm^{-1}, ~477 cm^{-1}, and ~548 cm^{-1} (Thibeau *et al*., 1978; de Faria *et al*., 1997; Hanesch, 2009; Das and Hendry, 2011). Bands at ~685 cm^{-1} and ~993 cm^{-1} were also noted by de Faria *et al.* (1997) and Hanesch (2009), which are consistent with the spectra in Fig. 4A. The bands at ~243 cm^{-1} and ~996 cm^{-1} are absent in Q-1, however Thibeau *et al*., (1978) also did not observe the 243 cm^{-1} band, and only de Faria *et al*. (1997) observed the ~993 cm^{-1} band.

Hematite was detected in Y-3 and CP-1 (Fig. 4B). In Y-3 bands were detected at ~217 cm^{-1} (strong), 290 cm^{-1} (strong), and 396 cm^{-1} (strong). In CP-1 bands were detected at ~222 cm^{-1} (strong), 246 cm^{-1} (weak), 295 cm^{-1} (strong), 408 cm^{-1} (very strong), 499 cm^{-1} (weak), and 608 cm^{-1} (strong). These values correspond with previously published values where bands were noted at ~225 cm^{-1}, ~245 cm^{-1}, ~290 cm^{-1}, ~411 cm^{-1}, ~496 cm^{-1}, and ~612 cm^{-1} (Thibeau *et al*., 1978; de Faria *et al*., 1997; Mazzetti and Thistlethwaite, 2002; Hanesch, 2009; Das and Hendry, 2011). The bands at ~217 cm^{-1} and ~396 cm^{-1} in Y-3 are consistent with those reported by Mazzetti and Thistlethwaite (2002), but are lower than other reported values. However, de Faria *et al.* (1997) noted that the band positions shift to lower wavenumbers at higher laser power, and Mazzetti and Thislethwaite (2001) observed spectra consistent with Y-3 by repeatedly scanning and subsequently transforming ferrihydrite and schwertmannite to hematite.

3.2.2 Sulfates

Sulfates show a strong band at ~1000 cm^{-1} due to symmetric stretching of the sulfate (SO_4^{2-}) ion (White, 2009). The position of this band determines which sulfate mineral is present. The SO_4^{2-} vibrational band occurs at ~988 cm^{-1} in barite, ~1008 cm^{-1} in gypsum, ~1006 – 1015 cm^{-1} in jarosite, ~1017 cm^{-1} in anhydrite, and ~1026 – 1038 cm^{-1} in alunite (Serna *et al*., 1986; Chio *et al*., 2005; Frost *et al*., 2006a; Frost *et al*., 2006b; White, 2009).

Gypsum was detected in CP-1 (Fig. 4C), with bands at ~414 cm^{-1} (weak), ~492 cm^{-1} (weak), ~620 cm^{-1} (weak), ~670 cm^{-1} (weak), ~1008 cm^{-1} (very strong), ~1136 cm^{-1} (weak), ~3401 cm^{-1} (weak), and ~3491 cm^{-1} (strong). These values correspond with previously published values where bands were noted at ~416 cm^{-1},

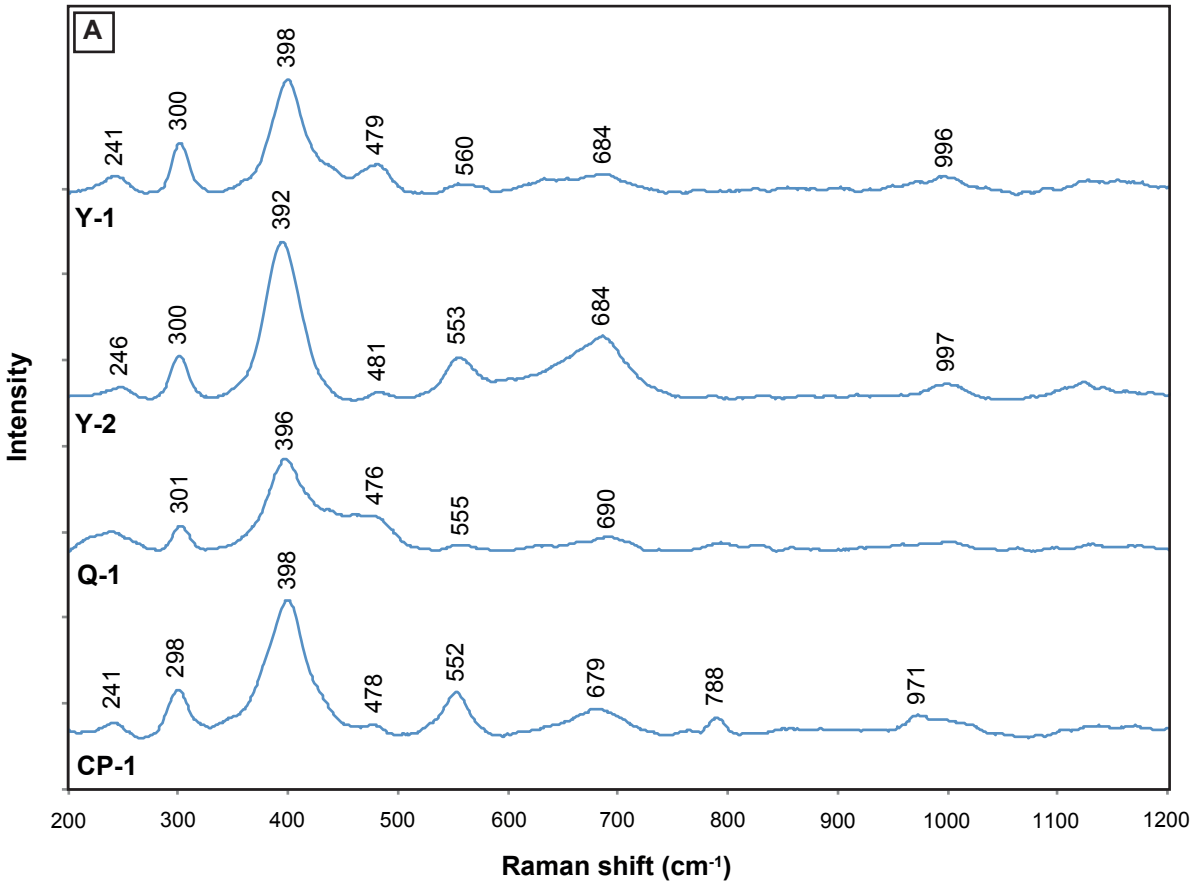

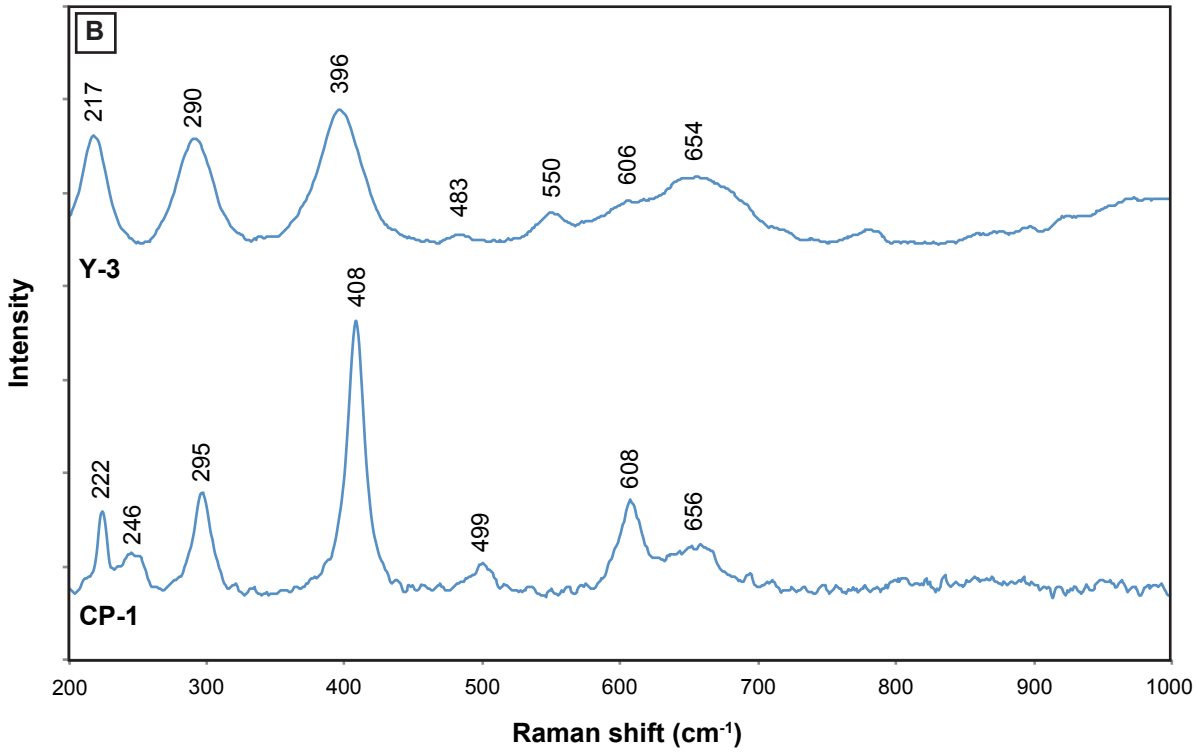

Figure 4 (continued over page)

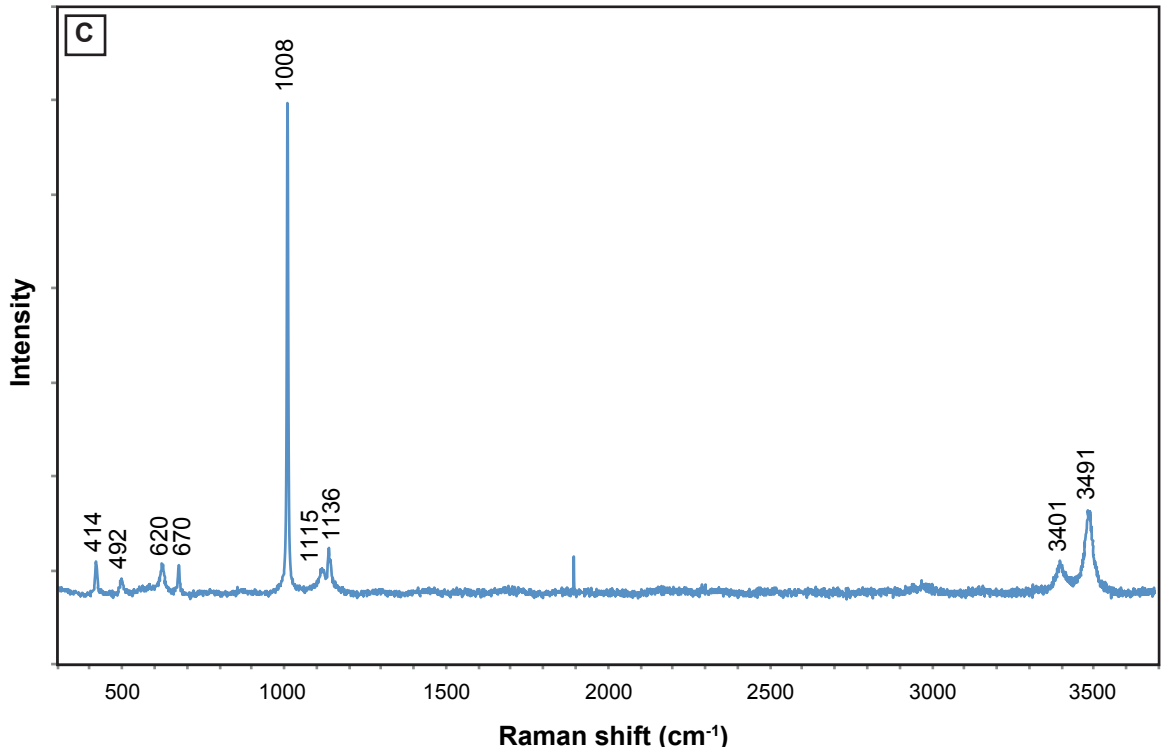

Figure 4 (continued over page)

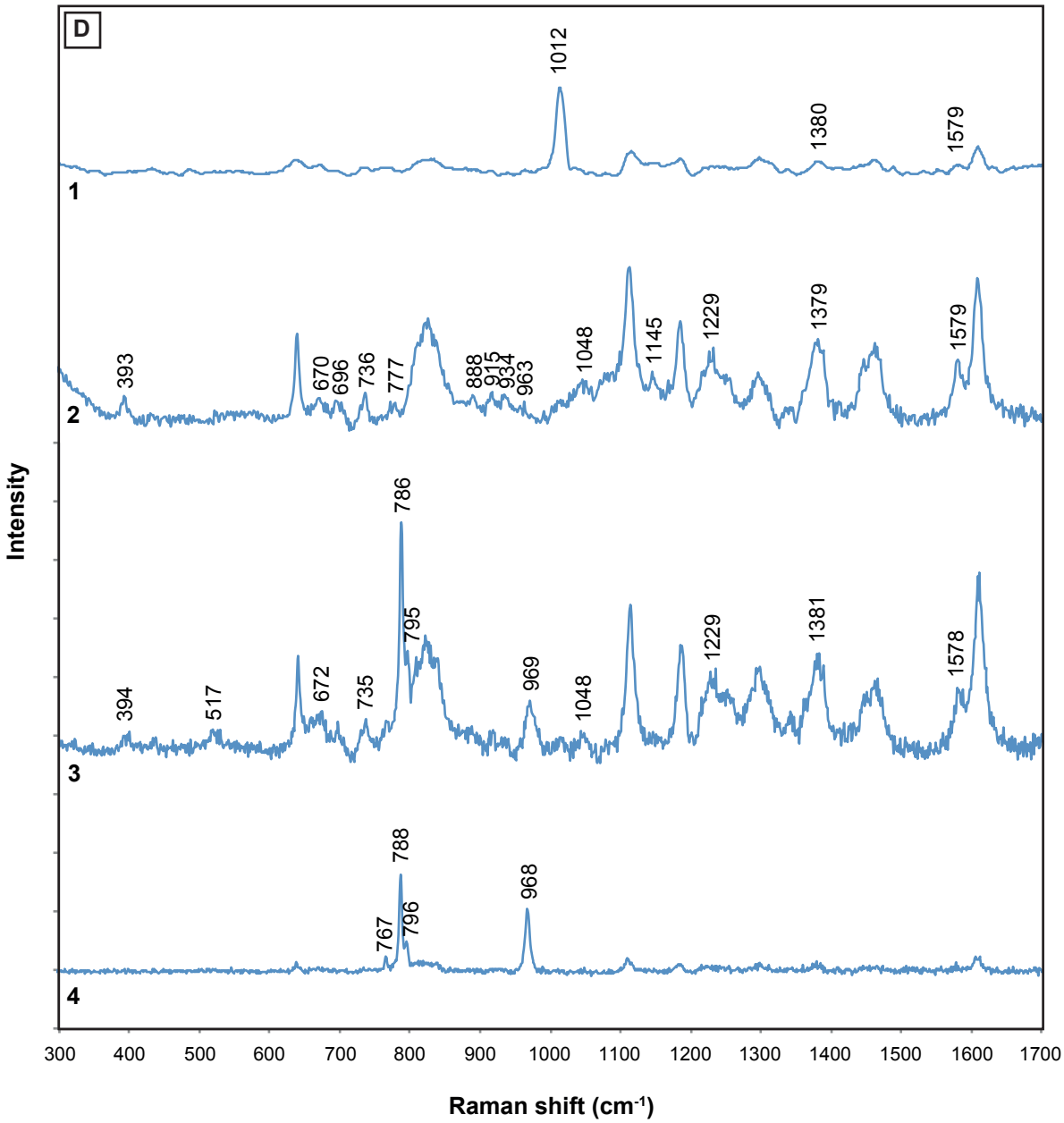

Figure 4. *Raman spectra of minerals detected in Y-1, Y-2, Q-1, Q-2, and CP-1. (A) Goethite spectra with labelled band positions for samples Y-1, Y-2, Q-1, and CP-1. (B) Hematite spectra with labelled band positions for samples Y-3 and CP-1. (C) Gypsum spectrum with labelled band positions for sample CP-1. (D) Sulfate spectra for sample CP-1. Unlabelled bands are due to the epoxy on the slide. 1: Possible jarosite spectrum; 2,3: Alunite spectra; 4: Possible barite spectrum.*

~494 cm^{-1}, ~620 cm^{-1}, ~671 cm^{-1}, ~1008 cm^{-1}, ~1136 cm^{-1}, ~3404 cm^{-1}, and ~3492 cm^{-1} (Berenblut *et al.*, 1971; Sarma *et al.*, 1998; Edwards *et al.*, 2005; White, 2009).

A putative sulfate was detected in CP-1, with a strong band at ~1012 cm^{-1}, suggesting jarosite (Fig. 4D-1). All other bands can be attributed to the epoxy on the slide. The lack of other bands not associated to the epoxy does not allow conclusive identification of this sulfate.

Another sulfate was detected in CP-1, with weak bands at ~393 cm^{-1}, ~777 cm^{-1}, ~963 cm^{-1}, ~1048 cm^{-1}, and 1229 cm^{-1} (Fig. 4D-2). These values correspond with previously published values for potassium alunite where bands were noted at 388.7 cm^{-1}, 773.3 cm^{-1}, 961.0 cm^{-1}, 1049 cm^{-1}, and 1228.4 cm^{-1} (Frost *et al.*, 2006a). A band at ~481 – 491 cm^{-1} has been reported (Serna *et al.*, 1986; Frost *et al.*, 2006a) but was not detected in our spectra. Other spectra from CP1 have an additional band at ~517 cm^{-1} (Fig. 4D-3), which can also be attributed to alunite (Serna *et al.*, 1986; Buzgar *et al.*, 2009). This band was not detected by Frost *et al.* (2006a).

Some spectra do not exhibit the SO_4^{2-} band at ~1049 cm^{-1}, however do have a band at ~969 cm^{-1} (Fig. 4D-4) also attributed to symmetrical stretching of the sulfate ion (Niaura and Malinauskas, 1998). A sulfate band at ~988 cm^{-1} is characteristic of barite (Edwards *et al.*, 2007; White, 2009).

3.3 Element geochemistry across opal veins

LA-ICP-MS analyses were undertaken across different coloured zones in opal veins: (1) the vein wall (brown material), identified as iron oxide/oxyhydroxide via VNIR-SWIR and Raman spectroscopy; (2) yellow material identified adjacent to the vein wall and within opal; (3) white material adjacent to precious opal; and (4) blue precious opal. Although 51 elements were analysed, gold was omitted because the reading was below the limit of detection for all targets. Silica was also omitted.

3.3.1 Trace element abundances

The average abundances for the four groups are shown in Table 2 and Fig. 5A-D. The vein wall is characterised by high concentrations of Fe, up to an average of 219358 ppm. The next most abundant elements are Al, Mn, and P, with average concentrations in the thousands of ppm, followed by Na, Mg, K, Ti, V, Cu, and Zn, with average concentrations in the hundreds of ppm. The yellow zone is characterised by Fe concentrations up to 73053 ppm, Al concentrations up to 10120 ppm, and Na concentrations up to 9265 ppm. Calcium and P have average concentrations in the thousands of ppm, followed by K and Mg with concentrations in the hundreds of ppm. The standard deviation for Fe is up to 119%, and <60% for other elements indicating a high degree of inhomogeneity in the yellow zone. The white zone is characterised by Na concentrations with an average up to 13646 ppm. Aluminium, K, and Ca, have concentrations in the

Table 2. *Average element abundances for different zones in samples Q-1, Q-2, Y-2, and Y-3. The concentrations are in ppm with % relative standard deviation.*

Sample	*Q-1*						*Q-2*				*Y-2*						*Y-3*			
Target	*Vein wall*		*Blue opal*		*Yellow material*		*Blue opal*		*Yellow material*		*Vein wall*		*Yellow material*		*White material*		*Vein wall*		*White material*	
	Average ppm	*RSD (%)*	*Average ppm*	*RSD (%)*	*Average ppm*	*RSD (%)*	*Average ppm*	*RSD (%)*	*Average ppm*	*RSD (%)*	*Average ppm*	*RSD (%)*	*Average ppm*	*RSD (%)*	*Average ppm*	*RSD (%)*	*Average ppm*	*RSD (%)*	*Average ppm*	*RSD (%)*
Na	769.63	12	6298.31	14	7428.64	5	8544.79	13	9265.68	18	860.50	17	7937.46	5	6582.63	9	848.87	5	13646.27	21
Mg	713.83	19	214.80	14	353.40	5	260.14	7	281.00	16	864.38	18	496.60	42	321.63	10	879.17	3	255.80	9
Al	7261.17	22	2904.20	8	6504.80	3	3475.71	8	5397.00	44	4855.46	36	10120.40	10	5027.50	8	2273.25	8	4403.50	6
P	1733.83	12	<LOD	-	662.50	27	49.00	-	1533.25	56	1488.77	6	1613.40	62	31.86	25	1495.50	4	99.80	11
K	318.42	64	1804.50	20	615.70	11	1282.14	25	708.25	19	95.85	42	792.00	34	930.75	28	149.08	29	2758.30	19
Ca	1255.08	11	<LOD	-	1262.00	16	1074.50	29	1257.25	16	978.92	17	1453.80	32	1138.00	15	635.58	12	1147.40	24
Ti	880.08	186	14.00	-	55.90	33	12.26	40	92.27	82	99.69	76	194.90	41	6.22	65	32.25	18	12.93	23
Fe	214053.03	4	80.67	32	22955.50	31	128.33	31	34081.50	119	219358.01	5	73053.00	60	86.25	26	225195.28	0	1440.00	15
Mn	2620.98	13	18.30	16	33.00	8	27.71	8	32.75	7	3498.25	14	96.10	60	15.38	15	4578.35	8	11.80	19
B	25.17	11	<LOD	-	<LOD	-	<LOD	-	6.50	-	23.54	14	7.53	51	<LOD	-	12.58	16	16.00	30
Sc	15.83	11	13.40	19	6.54	9	10.98	21	10.14	39	15.46	11	15.53	46	6.78	18	16.60	29	6.18	9
V	122.25	22	<LOD	-	13.41	34	<LOD	-	36.25	44	335.54	26	80.70	37	<LOD	-	220.17	13	0.98	17
Cr	89.25	11	<LOD	-	<LOD	-	11.00	-	6.57	24	590.62	28	16.53	68	<LOD	-	82.25	4	6.39	11
Co	71.67	14	0.50	12	0.58	19	0.85	25	1.11	36	80.62	15	10.35	55	0.41	22	16.17	23	0.34	19
Ni	84.50	13	<LOD	-	2.59	25	<LOD	-	6.16	43	97.08	14	31.10	59	3.50	26	18.00	21	10.75	53
Cu	207.42	15	10.70	19	22.20	18	19.57	26	30.50	57	188.31	9	88.90	66	16.00	32	194.00	5	27.30	39
Zn	366.83	11	5.82	80	5.59	24	4.46	32	12.27	111	249.92	13	52.50	37	9.55	34	104.58	17	14.30	33
Ga	10.89	14	0.41	-	0.25	18	0.37	36	0.49	48	7.52	33	1.34	51	0.24	5	1.38	10	0.25	5
Ge	2.20	37	<LOD	-	<LOD	-	<LOD	-	1.66	42	1.17	13	1.32	18	<LOD	-	1.56	16	<LOD	-
Y	11.32	17	0.54	27	1.64	12	0.72	26	2.59	85	8.99	8	7.25	52	0.78	9	6.38	19	0.85	12
Zr	148.09	315	15.50	22	6.37	27	20.00	18	12.03	21	6.23	101	10.65	16	16.88	14	6.27	15	11.60	9
Nb	1.20	233	<LOD	-	0.07	25	<LOD	-	0.11	17	0.13	35	0.54	53	<LOD	-	0.18	19	0.06	-
Sn	0.31	38	<LOD	-	<LOD	-	<LOD	-	0.37	-	0.16	18	<LOD	-	<LOD	-	0.14	11	0.99	33
Hf	2.31	296	1.12	38	0.35	43	1.48	25	0.81	35	0.16	118	0.51	32	1.36	33	0.09	22	0.47	37
Ta	0.10	201	<LOD	-	<LOD	-	<LOD	-	<LOD	-	0.01	10	<LOD	-	0.06	19	<LOD	-	<LOD	-
Pb	11.57	39	<LOD	-	0.36	26	0.66	-	1.83	43	8.32	29	5.76	57	0.24	27	1.65	30	0.75	62
Bi	0.03	24	3.38	-	0.15	-	<LOD	-	0.05	-	0.03	51	<LOD	-	<LOD	-	0.06	89	1.72	146
Li	1.38	19	<LOD	-	<LOD	-	3.22	-	1.41	-	0.97	34	1.71	12	<LOD	-	0.73	18	1.35	-
Rb	1.42	56	19.20	8	2.91	43	23.29	18	12.65	88	0.35	62	2.68	24	6.75	79	0.35	21	9.52	9
Cs	0.14	40	1.64	18	0.75	16	1.57	19	1.09	-	0.06	55	0.53	21	1.23	33	0.03	30	1.24	7
Be	6.62	32	<LOD	-	7.21	16	<LOD	-	12.00	24	3.68	17	12.25	10	<LOD	-	3.87	36	<LOD	-
Sr	240.83	120	18.90	13	44.20	2	28.57	9	36.50	35	40.08	26	49.40	14	35.63	6	20.00	10	31.30	9
Ba	150.58	41	54.50	12	118.30	4	87.57	13	89.13	26	31.00	45	99.30	21	90.38	3	13.58	6	76.40	17
La	25.20	91	0.16	37	0.35	20	0.18	27	0.47	99	1.74	16	0.68	41	0.17	18	1.83	17	0.42	50
Ce	42.58	89	1.36	60	1.30	6	1.12	22	1.72	76	4.05	11	2.42	38	1.00	10	5.39	11	1.40	29
Pr	4.12	86	0.13	9	0.18	13	0.23	66	0.34	64	0.56	7	0.44	34	0.11	10	0.62	14	0.15	31
Nd	14.88	79	0.73	-	0.99	13	0.89	85	1.92	57	2.86	4	2.62	34	0.62	24	3.04	15	0.54	27
Sm	2.59	64	<LOD	-	0.30	25	<LOD	-	0.81	32	0.94	11	0.90	49	0.24	3	1.00	14	<LOD	-
Eu	0.65	58	<LOD	-	0.10	17	<LOD	-	0.22	30	0.32	9	0.33	51	0.08	2	0.29	12	0.07	-
Gd	2.28	53	0.93	-	0.46	28	<LOD	-	1.11	62	1.12	12	1.32	50	<LOD	-	1.14	14	0.31	10
Tb	0.29	34	<LOD	-	0.06	37	<LOD	-	0.23	45	0.19	15	0.26	54	0.05	-	0.18	17	0.04	-
Dy	1.76	33	<LOD	-	0.40	25	<LOD	-	1.38	20	1.39	10	1.79	61	0.27	-	1.21	17	0.29	10
Ho	0.37	23	<LOD	-	0.08	30	<LOD	-	0.26	27	0.32	8	0.38	56	<LOD	-	0.24	16	0.05	-
Er	1.12	22	<LOD	-	0.24	30	<LOD	-	0.88	41	1.09	10	1.26	61	<LOD	-	0.80	28	0.18	-
Tm	0.16	21	<LOD	-	0.05	31	<LOD	-	0.13	58	0.17	12	0.19	51	0.06	-	0.12	18	<LOD	-
Yb	1.09	37	<LOD	-	0.32	33	<LOD	-	1.32	38	1.14	11	1.53	51	<LOD	-	0.82	28	<LOD	-
Lu	0.19	36	<LOD	-	0.07	42	<LOD	-	0.20	47	0.20	13	0.29	40	<LOD	-	0.14	21	<LOD	-
Th	5.90	38	<LOD	-	0.12	23	<LOD	-	0.28	40	1.30	113	0.84	57	<LOD	-	0.10	91	<LOD	-
U	1.07	46	<LOD	-	0.28	50	<LOD	-	1.09	37	1.01	16	1.27	73	<LOD	-	1.72	8	0.12	8

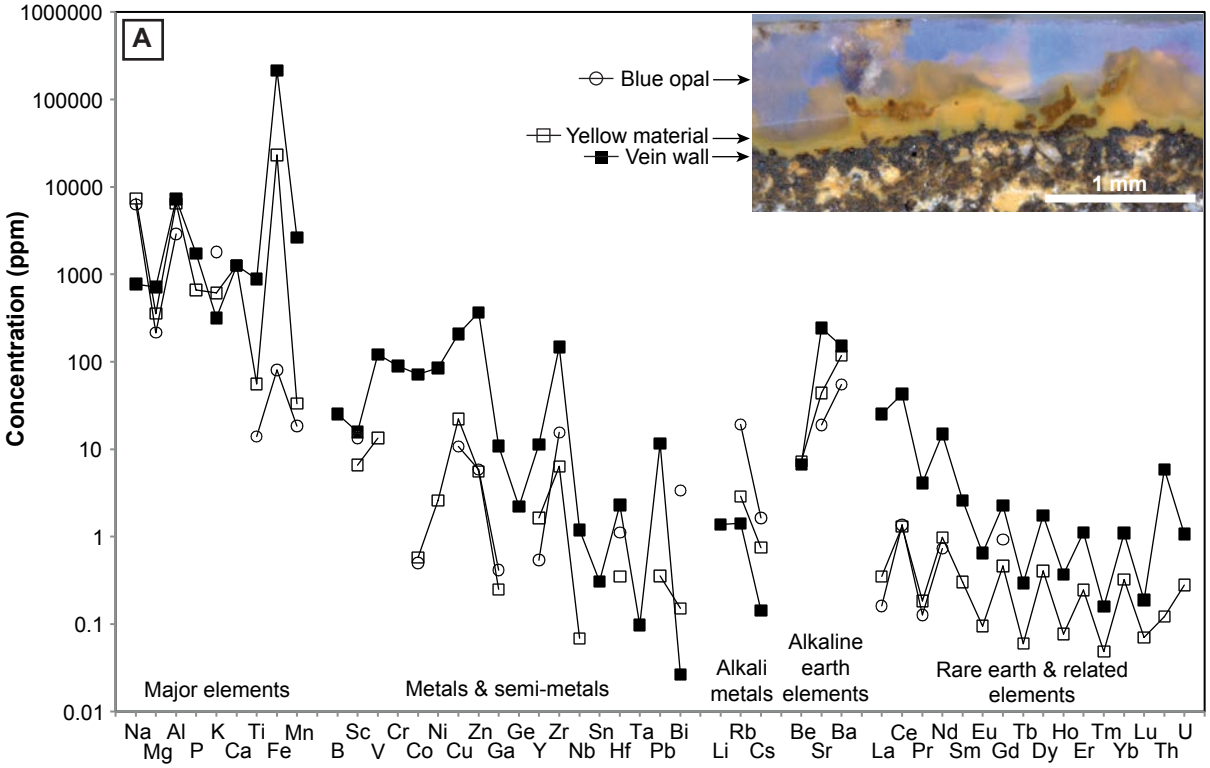

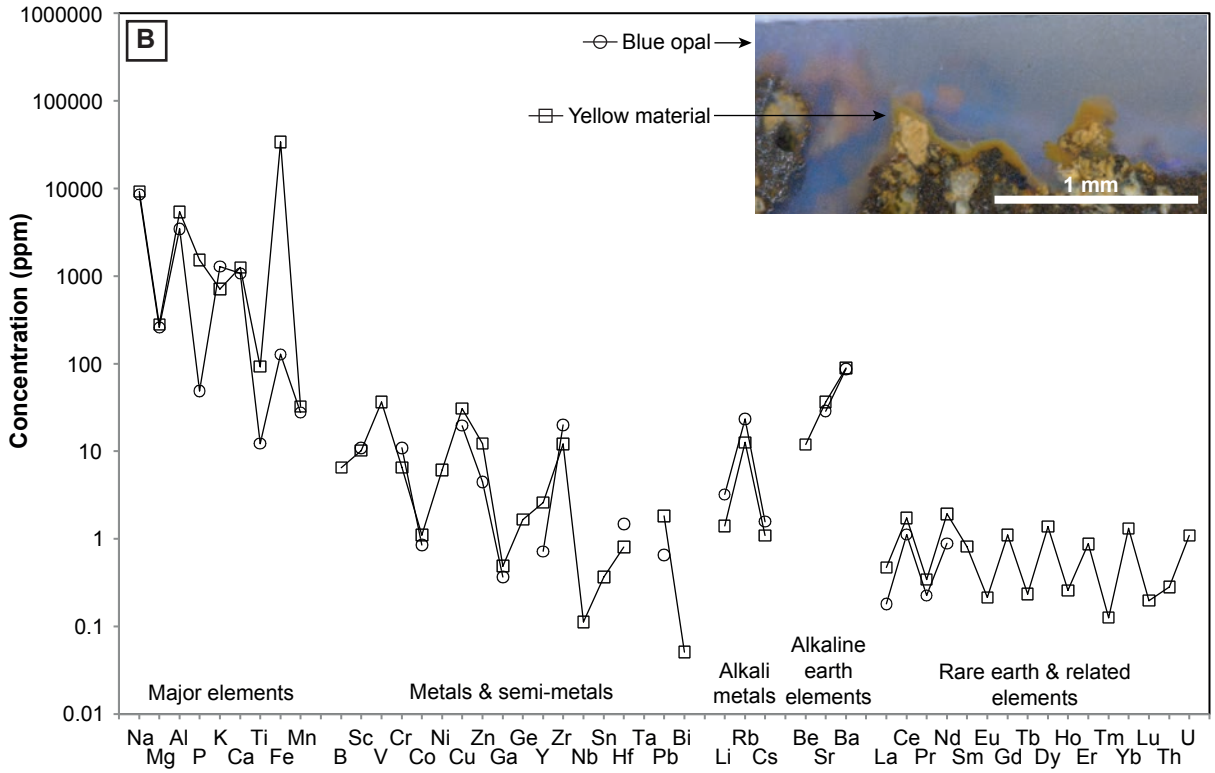

Figure 5 (continued over page)

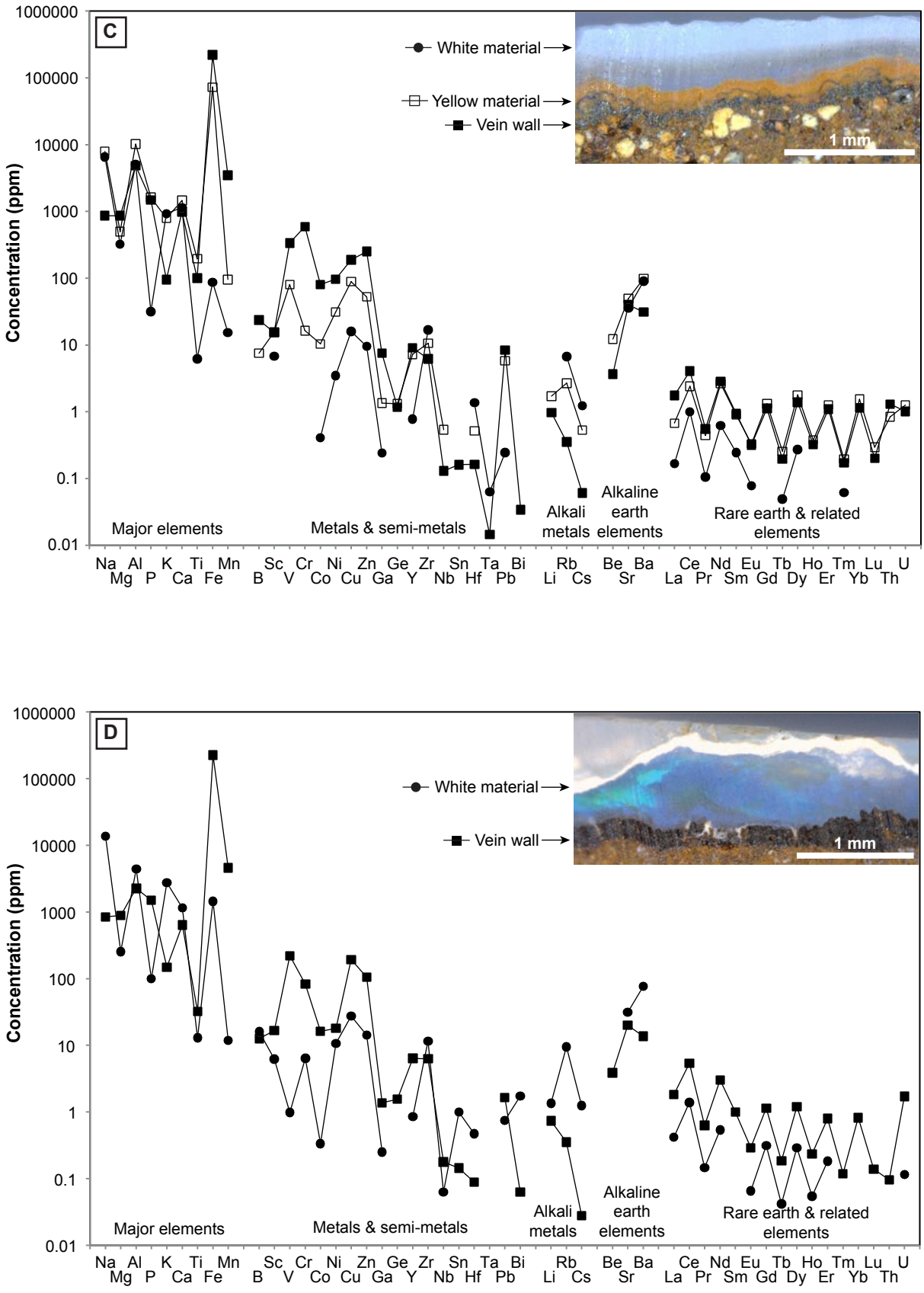

Figure 5. *Average values for the elemental abundances within each zone with photos of samples. (A) Q-1, (B) Q-2, (C) Y-2, (D) Y-3.*

thousands of ppm, and Mg in the hundreds of ppm. The blue opal has Na, Al, and K in concentrations in the thousands of ppm, and Mg in the hundreds of ppm. The rare earth and related elements have very low concentrations mostly less than 5 ppm, however, in the blue opal these elements are below the limit of detection. In all zones Ba generally has a concentration <100 ppm, indicating a volcanic origin for the opals (Gaillou *et al*., 2008). Dutkiewicz *et al*. (2015) suggested that this might be due to the volcaniclastic host rocks in the GAB.

4. Main findings and implications for Martian weathering

This is the first detailed study on mineral assemblages preserved as inclusions in opal veins from central Australia. Minerals were documented via VNIR-SWIR and Raman spectroscopy and include Al-rich phyllosilicates (kaolinite/halloysite, montmorillonite), iron oxides and oxyhydroxides (hematite, goethite, maghemite, ferrihydrite, and possibly schwertmannite), and sulfates (gypsum, alunite, and possibly barite and jarosite). These minerals, co-genetic with opaline silica since fossilised in opal veins, have been protected from *ca.* 60 myr of weathering in an arid and stable landscape, following the drying out of central Australia between 95 and 60 Ma (e.g. Rey, 2013). No opal deposits have been found in Cenozoic to recent lithologies of the GAB, therefore it is likely that opal production had ceased by *ca.* 65 Ma (Rey, 2013).

4.1 Description of mineral assemblages

The five opal samples from Yowah and Quilpie came from the Winton Formation (*ca.* 97 – 93 Ma; deposited in fluvial environments during sea regression and predominantly composed of coarse volcaniclastic sandstones, mudstones, and pyritic shales; Exon and Senior, 1976), whereas the sample from Coober Pedy came from the Bulldog Shale (*ca.* 125 – 113 Ma; deposited in a shallow marine environment and predominantly siltstones and pyritic mudstones with minor sandstones; Exon and Senior, 1976). The mineralogical assemblages identified in each sample are summarised in Table 3. Iron oxides/oxyhydroxides were identified in every vein. Inclusions of phyllosilicates were only identified in samples from Yowah and Quilpie. However, phyllosilicates are common in the walls of opal veins, so have been included in the mineral assemblage for CP-1. Inclusions of sulfates were only identified in the vein from Coober Pedy. The variations in mineralogy between the samples from the Winton Formation and the Bulldog Shale may be due to small variations in their host rock lithologies, or variations in environmental conditions (e.g., pH, water to rock ratio, temperature).

The mineralogical assemblage common to all opal fields is opal, goethite, and kaolinite/halloysite. Rey (2013) summarised a series of reactions in which kaolinite can transform to goethite and opal in the presence of ferric iron in acidic solution. The pH of this acidic solution determined minerals formed during opalisation. Figure 6 shows the pH ranges at which minerals have been found. Goethite, common to all samples, has been found in environments with pH 2.5 – 7.5 (Bigham *et al*., 1992). Goethite has been found

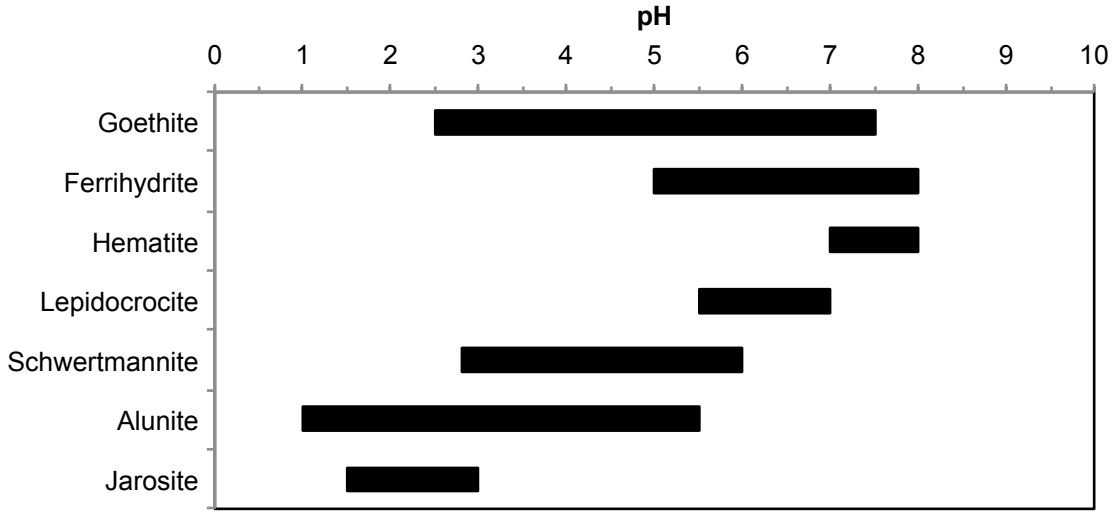

Figure 6. *Graph showing the range of pH at which iron oxides/oxyhydroxides and sulfates form. (Goethite: Bigham* et al.*, 1992; Murad and Rojík, 2004. Ferrihydrite: Bigham* et al.*, 1992; Bigham* et al.*, 1996; Murad and Rojík, 2004. Hematite: Schwertmann and Murad, 1983. Lepidocrocite: Jönnson* et al.*, 2006. Schwertmannite: Bigham* et al.*, 1994; Bigham* et al.*, 1996; Schwertmann* et al.*, 1995. Alunite: Rayot* et al.*, 1992; Wray, 2011. Jarosite: Bigham* et al.*, 1992; Rayot* et al.*, 1992; Murad and Rojík, 2004; Hayes* et al.*, 2014.)*

with ferrihydrite (as in sample Q-1) at pH 5 – 7 (Murad and Rojík, 2003), and found with ferrihydrite, lepidocrocite, and schwertmannite (as in sample Y-1) at a pH ~5.5 in acid mine drainage environments (Jönnson *et al*., 2006). Lepidocrocite can also form at neutral pH (Jönnson *et al*., 2006), therefore a mineral assemblage of goethite, hematite, ferrihydrite, and lepidocrocite without schwertmannite could indicate a near neutral pH. The pH at which hematite is found (Fig. 6) suggests that hematite and goethite can co-precipitate at neutral pH (as in samples Y-2 and Y-3). Alunite and Jarosite are known to co-precipitate during acidic evaporitic processes (Long *et al*., 1992), which is consistent with the abundance of gypsum in the Coober Pedy region (Bird *et al*., 1989). If both alunite and jarosite are present in CP-1 the pH during mineral precipitation was between 1.5 and 3. Jarosite, however, has not been definitively identified, therefore the pH during CP-1 formation could have been in the range 1 – 5.5. Hence, opal veins from both the Winton Formation and Bulldog Shale record mineral assemblages that point to acidic conditions commonly reported in acid mine drainage environments where acidic oxidative conditions prevail.

Table 3. *Mineral assemblages identified in opal veins.*

		Y-1	**Y-2**	**Y3**	**Q-1**	**CP-1**
		Winton Formation				Bulldog shale
Precious opal		X	X	X	X	X
Common opal						X
Iron oxides / oxyhydroxides	Goethite	X	X	X	X	X
	Ferrihydrite	X			?	
	Hematite	X	X	X		X
	Lepidocrocite	X				
	Schwertmannite	?				
	Maghemite			X		
Phyllosilicates	Kaolinite	X	X	X	X	X
	Halloysite	X	X	X	X	X
	Montmorillonite	X	X		X	X
Sulphates	Gypsum					X
	Alunite					X
	Jarosite					?
	Barite					?

4.2 Implications for weathering on Mars

Interestingly, the groups of minerals documented in this study, including opaline silica, have been identified via orbital spectroscopy as co-existing on Mars (e.g. Gendrin *et al*., 2005; Poulet *et al*., 2005; Mustard *et al*.,

2008; Ehlmann *et al*., 2009; McKeown *et al*., 2009; Carter *et al*., 2013). Table 4 summarises the minerals detected in various regions on Mars. Note, barite has not been detected on Mars and the presence of schwertmannite has not been confirmed. Similarly to the GAB, the surface of Mars has recorded a period of dehydration (*ca.* 3.7 Ga), followed by protracted weathering in an arid and stable landscape. Unlike the GAB, however, mineral formation on Mars is generally attributed to three stages: (1) phyllosilicates during the wet Noachian (*ca.* 4.1 – 3.7 Ga); (2) sulfates during the acidic Hesperian (*ca.* 3.7 – 2.9 Ga); and (3) iron oxides during the arid Amazonian (*ca.* 2.9 Ga to present) (Chevrier *et al*., 2007; Chevrier and Mathe, 2007; Hurowitz and McLennon, 2007; Milliken *et al*., 2008; Mustard *et al*., 2008; Ehlmann *et al*., 2011). However, this study on opal veins from central Australia suggests that these minerals can form concurrently in acidic conditions, given the low-pH required for the formation of most of the minerals present, and may have formed during the Noachian to Hesperian on Mars.

Table 4. *Minerals identified in specific regions on Mars (Hamilton* et al*., 2001; Ming* et al*., 2006; Wang* et al*., 2006; Clark* et al*., 2007; Le Deit* et al*., 2008; Milliken* et al*., 2008; Ehlmann* et al*., 2009; Farrand* et al*., 2009).*

		Mawrth Vallis	**Nili Fossae**	**Valles Marineris**	**Gusev Crater**
Opaline Silica		X	X	X	X
Iron oxides / oxyhydroxides	Goethite	X		X	X
	Ferrihydrite	X		X	
	Hematite		X		X
	Lepidocrocite				
	Schwertmannite	?			
	Maghemite				
Phyllosilicates	Kaolinite	X	X	X	?
	Halloysite		X		?
	Montmorillonite	X	X	X	X
Sulphates	Gypsum			X	
	Alunite				
	Jarosite	X	X	X	X
	Barite				

The weathering history in central Australian between *ca*. 95 and 60 Ma is preserved in millimetre-scale opal veins. This weathering history is remarkably similar to that of Mars at the time when the red planet dried out. It involves a rare and long-lived oxidative acidic condition (pH < 5.5) at a regional scale. This study shows that central Australia is an unparalleled terrestrial analogue for Mars. Furthermore,

colonies of microbes have been reported in inclusions in opal veins from central Australia (Watkins *et al*., 2011). This study suggests that the microbes identified could survive in pH < 5.5, lower than the near neutral pH Watkins *et al*. (2011) proposed. Additionally, the most abundant elements found in opals (Si, Fe, Mg, Al, Na, K and Ca) are among the most abundant elements in the Martian crust (e.g. Hahn, 2009). Hence, if life ever existed on Mars, opals in central Australia may hold the key to finding it.

Acknowledgements

This project was made possible thanks to the Dr. Eduard Gübelin Research Scholarship 2014 and the Australian Research Council Discovery Grant DP0987604. Thanks to Klemens Link for his assistance with the LA-ICP-MS and processing the data and the expertise supplied by the Gübelin Gem Laboratory in Lucerne, Switzerland. Thanks to Elizabeth Carter and Joonsup Lee at the Vibrational Spectroscopy Core Facility at the University of Sydney for their help with Raman spectroscopy, and to Richard Murphy at the Rio Tinto Centre for Mine Automation for the use of his VNIR-SWIR instrument. Lastly, thanks to Associate Professor Patrice Rey at the University of Sydney for his advice and support throughout this project.

References

Berenblut, B. J., Dawson, P. and Wilkinson, G. R. (1971): The Raman spectrum of gypsum, *Spectrochimica Acta* **27A**, 1849-1863.

Bigham, J. M., Carlson, L. and Murad, E. (1994): Schwertmannite, a new iron oxyhydroxy-sulphate from Pyhäsalmi, Finland, and other localities, *Mineralogical Magazine* **58**, 641-648.

Bigham, J. M., Schwertmann, U. and Carlson, L. (1992): Mineralogy of precipitates formed by the biogeochemical oxidation of Fe(II) in mine drainage, *Catena* **21**, 219-232.

Bigham, J. M., Schwertmann, U. Traina, S. J., Winland, R. L. and Wolf, M. (1996): Schwertmannite and the chemical modeling of iron in acid sulfate waters, *Geochimica et Cosmochimica Acta* **60**(12), 2111-2121.

Bird, M. I., Andrew, A. S., Chivas, A. R. and Lock, D. E. (1989): An isotopic study of surficial alunite in Australia: 1. Hydrogen and sulfur isotopes, *Geochimica et Cosmochimica Acta* **53**, 3223-3237.

Bishop, J. L. and Murad, E. (1996): Schwertmannite on Mars? Spectroscopic analyses of schwertmannite, its relationship to other ferric minerals, and its possible presence in the surface material on Mars, *In* Dyar, M. D., McCammon, C. and Schaefer, M. W. (eds) *Mineral Spectroscopy: A Tribute to Roger G. Burns, The Geochemical Society, Houston, 337-358.*

Bishop, J. L., Murad, E. and Dyar, M. D. (2015): Akaganéite and schwertmannite: Spectral properties and geochemical implications of their possible presence on Mars, *American Mineralogist* **100**, 738-746.

Bishop, J. L., Pieters, C. M. and Burns, R. G. (1993): Reflectance and Mössbauer spectroscopy of ferrihydrite-montmorillonite assemblages as Mars soil analog materials, *Geochimica Cosmochimica Acta* **57**, 4583-4595.

Bishop, J. L., Pieters, C. M., Burns, R. G., Edwards, J. O., Mancinella, R. L. and Fröschl, H. (1995): Reflectance Spectroscopy of Ferric Sulfate-Bearing Montmorillonites as Mars Soil Analog Materials, *Icarus* **117**, 101-119.

Buzgar, N., Buzatu, A. and Sanislav, I. V. (2009): The Raman study on certain sulfates, *Geologie. Tomul LV, nr. 1*.

Carter, J., Poulet, F., Bibring, J.-P., Mangold, N. and Murchie, S. (2013): Hydrous minerals on Mars as seen by the CRISM and OMEGA imaging spectrometers: Updated global view, *Journal of Geophysical Research: Planets* **118**, 831-858.

Chevrier, V. and Mathé, P.E. (2007): Mineralogy and evolution of the surface of Mars: A review, *Planetary and Space Science* **55**, 289-314.

Chevrier, V., Poulet, F. and Bibring, J.-P. (2007): Early geochemical environment of Mars as determined from thermodynamics of phyllosilicates, *Letters to Nature* **448**, 60-63.

Chio, C. H., Sharma, S. K. and Muenow, D. W. (2005): Micro-Raman studies of hydrous ferrous sulfates and jarosites, *Spectrochimica Acta Part A* **61**, 2428-2433.

Clark III, B. C., Arvidson, R. E., Gellert, R., Morris, R. V., Ming, D. W., Richter, L., Ruff, S. W., Michalski, J. R., Farrand, W. H., Yen, A., Herkenhoff, K. E., Li, R., Squyres, S. W., Schröder, C., Klingelhöfer, G. and Bell III, J. F. (2007): Evidence for montmorillonite or its compositional equivalent in Columbia Hills, Mars, *Journal of Geophysical Research* **112**.

Clark, R. N., King, T. V. V., Klejwa, M. and Swayze, G. A. (1990): High Spectral Resolution Reflectance Spectroscopy of Minerals, *Journal of Geophysical Research* **95**(B8), 12653-12680.

Cuadros, J. and Michalski, J. R. (2013): Investigation of Al-rich clays on Mars: Evidence for kaolinite-smectite mixed-layer versus mixture of end-member phases, *Icarus* **222**, 296-306.

Das, S. and Hendry M. J. (2011): Application of Raman spectroscopy to identify iron minerals commonly found in mine wastes, *Chemical Geology* **290**, 101-108.

De Faria, D. L. A., Silva, S. V. and de Oliveria, M. T. (1997): Raman Microscopy of Some Iron Oxides and Oxyhydroxides, *Journal of Raman Spectroscopy* **28**, 873-878.

Dutkiewicz, A., Langrebe, T. C. W. and Rey, P. F. (2015): Origin of silica and fingerprinting of Australian sedimentary opals, *Gondwana Research* **27**, 786-795.

Edwards, H. G. M., Jorge Villar, S. E., Parnell, J., Cockell, C. S. and Lee, P. (2005): Raman spectroscopic analysis of cyanobacterial gypsum halotrophs and relevance for sulfate deposits on Mars, *The Royal Society of Chemistry: Analyst* **130**, 917-923.

Ehlmann, B. L., Berger, G., Mangold, N., Michalski, J. R., Catling, D. C., Ruff, S. W., Chassefière, E., Niles, P. B., Chevrier, V. and Poulet, F. (2013): Geochemical Consequences of Widespread Clay Mineral Formation in Mars' Ancient Crust, *Space Science Review* **174**, 329-364.

Ehlmann, B. L., Mustard, J. F., Murchie, S. L., Bibring, J.-P., Meunier, A., Fraeman, A. A. and Langevin, Y. (2011): Subsurface water and clay mineral formation during the early history of Mars, *Nature Review* **479**, 53-60.

Ehlmann, B. L., Mustard, J. F., Swayze, G. A., Clark, R. N., Bishop, J. L., Poulet, F., Des Marais, D. J., Roach, L. H., Milliken, R. E., Wray, J. J., Barnouin-Jha, O. and Murchie, S. L. (2009), Identification of hydrated silicate minerals on Mars using MRO-CRISM: Geologic context near Nili Fossae and implications for aqueous alteration, *Journal of Geophysical Research* **114**.

Exon, N. F. and Senior, B. R. (1976): The Cretaceous of the Eromanga and Surat Basins, *BMR Journal of Australian Geology and Geophysics* **1**, 33-50.

Farrand, W. H., Glotch, T. D., Rice Jr., J. W., Hurowitz, J. A. and Swayze, G. A. (2009): Discovery of jarosite within the Mawrth Vallis region of Mars: Implications for the geologic history of the region, *Icarus* **204**, 478-488.

Frost, R. L., Wills, R.-A., Weier, M. L., Martens, W. and Kloprogge, J. T. (2006a): A Raman spectroscopic study of alunites, *Journal of Molecular Structure* **785**, 123-132.

Frost, R. L., Wills, R.-A., Weier, M. L., Martens, W. and Mills, S. (2006b): A Raman spectroscopic study of selected natural jarosites, *Spectrochimica Acta Part A* **63**, 1-8.

Gaillou, E., Delaunay, A., Rondeau, B., Bouhnik-le-Coz, M., Fritsch, E., Cornen, G. and Monnier, C. (2008): The geochemistry of gem opals as evidence of their origin, *Ore Geology Reviews* **34**, 113-126.

Gendrin, A., Mangold, N., Bibring, J.-P., Langevin, Y., Gondet, B., Poulet, F., Bonello, G., Quantin, C., Mustard, J., Arvidson, R. and LeMouélic, S. (2005): Sulfates in Martian Layered Terrains: The OMEGA/Mars Express View, *Science* **307**, 1587-1591.

Hahn, B. C. (2009): The Chemical Composition and Evolution of the Martian Upper Crust and Near Surface Environment, *Ph.D. Thesis, Stony Brook University*.

Hamilton, V. E., Christensen, P. R., McSween Jr., H. Y., Clark, R. N. and Hoefen, T. M. (2001): Spectral variations in MGS TES data of Nili Fossae: A possible source region for SNC meteorites on Mars? *Planetary Science XXXII*.

Hanesch, M. (2009): Raman spectroscopy of iron oxides and (oxy)hydroxides at low laser power and possible applications in environmental magnetic studies, *Geophysical Journal International* **177**, 941-948.

Hayes, S. M., Root, R. A., Perdrial, N., Maier, R. M. and Chorover, J. (2014): Surficial weathering of iron sulfide mine tailings under semi-arid climate, *Geochimica et Cosmochimica Acta* **141**, 240-257.

Hunt, G. R. (1977): Spectral signatures of particulate minerals in the visible and near infrared, *Geophysics* **42**(3), 501-513.

Hurowitz, J. A. and McLennon, S. M. (2007): A ~3.5 Ga record of water-limited, acidic weathering conditions on Mars, *Earth and Planetary Science Letters* **260**, 432-443.

Jönnson, J., Jönnson, J. and Lövgren, L. (2006): Precipitation of secondary Fe(III) minerals from acid mine drainage, *Applied Geochemistry* **21**, 437-445.

Le Deit, L., Le Mouélic, S., Bourgeois, O., Combe, J.-P., Mège, D., Sotin, C., Gendrin, A., Hauber, E., Mangold, N. and Bibring, J.-P. (2008): Ferric oxides in East Candor Chasma, Valles Marineris (Mars) inferred from analysis of OMEGA/Mars Express data: Identification and geological interpretation, *Journal of Geophysical Research* **113**.

Long, D. T., Fegan, N. E., Lyons, W. B., Hines, M. E. and Macumber, P. G. (1992): Formation of alunite, jarosite and hydrous iron oxides in a hypersaline system: Lake Tyrrell, Victoria, Australia, *Chemical Geology* **96**, 183-202.

Mazzetti, L. and Thistlethwaite, P. J. (2002): Raman spectra and thermal transformations of ferrihydrite and schwertmannite, *Journal of Raman Spectroscopy* **33**, 104-111.

McKeown, N. K., Bishop, J. L., Cuadros, J., Hillier, S., Amador, E., Makarewicz, H. D., Parente, M. and Silver, E. A. (2011): Interpretation of reflectance spectra of clay mineral-silica mixtures: Implications for Martian clay mineralogy at Mawrth Vallis, *Clays and Clay Minerals* **59**(4), 400-415.

McKeown, N. K., Bishop, J. L., Noe Dobrea, E. Z., Ehlmann, B. L., Parente, M., Mustard, J., Murchie, S. L., Swayze, G. A., Bibring, J.-P. and Silver, E. A. (2009): Characterization of phyllosilicates observed in the central Mawrth Vallis region, Mars, their potential formation processes, and implications for past climate, *Journal of Geophysical Research – Planets* **144**.

Milliken, R. E., Swayze, G. A., Arvidson, R. E., Bishop, J. L., Clark, R. N., Ehlmann, B. L., Green, R. O., Grotzinger, J. P., Morris, R. V., Murchie, S. L., Mustard, J. F. and Weitz, C. (2008): Opaline silica in young deposits on Mars, *Geology* **36**, 847-850.

Ming, D. W., Mittlefehldt, D. W., Morris, R. V., Golden, D. C., Gellert, R., Yen, A., Clark, B. C., Squyres, S. W., Farrand, W. H., Ruff, S. W., Arvidson, R. E., Klingelhöfer, G., McSween, H. Y., Rodionov, D. S., Schröder, C., de Souza Jr., P. A. and Wang, A. (2006): Geochemical and mineralogical indicators for aqueous processes in the Columbia Hills of Gusev crater, Mars, *Journal of Geophysical Research* **111**.

Morris, R. V., Lauer, H. V., Lawson, C. A., Gibson, E. K. Jn., Nace, G. A. and Stewart, C. (1985): Spectral and other physicochemical properties of submicron powders of hematite (α-Fe_2O_3), maghemite (γ-Fe_2O_3), magnetite (Fe_3O_4), goethite (α-FeOOH), and lepidocrocite (γ-FeOOH), *Journal of Geophysical Research* **90**, 3126-3144.

Murad, E. and Rojík, P. (2003): Iron-rich precipitates in a mine drainage environment: Influence of pH on mineralogy, *American Mineralogist* **88**, 1915-1918.

Murad, E. and Rojík, P. (2004): Jarosite, schwertmannite, goethite, ferrihydrite and lepidocrocite: the legacy of coal and sulfide ore mining, *SuperSoil 2004: 3rd Australian New Zealand Soils Conferences*.

Murphy, R. and Monteiro, S. T. (2013): Mapping the distribution of ferric iron minerals on a vertical mine face using derivative analysis of hyperspectral imagery (430–970 nm), *ISPRS Journal of Photogrammetry and Remote Sensing* **75**, 29-39.

Murphy, R., Schneider, S. and Monteiro, S. T. (2014): Consistency of Measurements of Wavelength Position From Hyperspectral Imagery: Use of the Ferric Ion Crystal Field Absorption at ~900 nm as an Indicator of Mineralogy, *IEEE Transactions on Geoscience and Remote Sensing* **52**(5), 2843-2857.

Mustard. J. F., Murchie, S. L., Pelkey, S. M., Ehlmann, B. L., Milliken, R. E., Grant, J. A., Bibring, J.-P., Poulet, F., Bishop, J., Noe Dobrea, E., Roach, L., Seelos, F., Arvidson, R. E., Wiseman, S., Green, R., Hash, C., Humm, D., Malaret, E., McGovern, J. A., Seelos, K., Clancy, T., Clark, R., Des Marais, D., Izenberg, N., Knudson, A., Langevin, Y., Martin, T., McGuire, P., Morris, R., Robinson, M., Roush, T., Smith, M., Swayze, G., Taylor, H., Titus, T. and Wolff, M. (2008): Hydrated silicate minerals on Mars observed by the Mars Reconnaissance Orbiter CRISM instrument, *Letters to Nature* **454**, 305-309.

Niaura, G. and Malinauskas, A. (1998): Surface-enchanced Raman spectroscopy of ClO_4^- and SO_4^{2-} anions adsorbed at a Cu electrode, *Journal of the Chemical Society, Faraday Transactions* **94**(15), 2205-2211.

Poulet, F., Bibring, J.-P., Mustard, J. F., Gendrin, A., Mangold, N., Langevin, Y., Arvidson, R. E., Gondet, B., Gomez, C. and the Omega Team (2005): Phyllosilicates on Mars and implications for early martian climate, *Nature Articles* **438**, 623-627.

Rayot, V., Self, P. and Thiry, M. (1992): Transition of clay minerals to opal-CT during ground-water silicification, Mineralogical and geochemical records of paleoweathering, Schmitt and Gall (eds.), ENSMP Memoire de Societe de la Terre **18**, 47-59.

Rey, P. (2013): Opalisation of the Great Artesian Basin (central Australia): an Australian story with a Martian twist, *Australian Journal of Earth Sciences: An International Geoscience Journal of the Geological Society of Australia* **60** (3), 291-314.

Roberts, G. E., Rey, P. F., Brand, H. E. A. and Singh, B. (2014): Alteration minerals in the Great Artesian Basin: Comparison to weathering processes on Mars, *Proceedings from 14th Australian Space Research Conference*, 87-98.

Sarma, L. P., Prasad, P. S. R. and Ravikumar, N. (1998): Raman Spectroscopic Study of Phase Transitions in Natural Gypsum, *Journal of Raman Spectroscopy* **29**, 851-956.

Schwertmann, U., Bigham, J. M. and Murad, E. (1995): The first occurrence of schwertmannite in a natural stream environment, *European Journal of Mineralogy* **7**, 547-552.

Schwertmann, U. and Murad, E. (1983): Effect of pH on the formation of goethite and hematite from ferrihydrite, *Clays and Clay Minerals* **31**, 277-284.

Senior, B. R. (1979): Mineralogy and chemistry of weathered and parent sedimentary rocks in southwest Queensland, *BMR Journal of Australian Geology & Geophysics* **4**, 111-124.

Serna, C. J., Parada Cortina, C. and Garcia Ramos, J. V. (1986): Infrared and Raman study of alunite-jarosite compounds, *Spectrochimica Acta* **42A** (6), 729-734.

Sherman, D. M., Burns, R. G. and Burns, V. M. (1982): Spectral characterization of the iron oxides with application to the martian bright region mineralogy, *Journal of Geophysics Research* **87**(B12), 10, 169-10, 180.

Simon-Coinçon, R., Milnes, A. R., Thiry, M. and Wright, M. J. (1996): Evolution of landscapes in northern South Australia in relation to the distribution and formation of silcretes, *Journal of the Geological Society, London* **153**, 467-480.

Taylor, G. and Shirtliff, G. (2003): Weathering: cyclical or continuous? An Australian perspective, *Australian Journal of Earth Sciences* **50**, 9-17.

Thibeau, R. J., Brown, C. W. and Heidersbach, R. H. (1978): Raman spectra of possible corrosion products of iron, *Applied Spectroscopy* **32**, 532-535.

Wang, A., Korotev, R. L., Jolliff, B. L., Haskin, L. A., Crumpler, L., Farrand, W. H., Herkenhoff, K. E., de Souza Jr., P., Kusack, A. G., Hurowitz, J. A. and Tosca, N. J. (2006): Evidence of phyllosilicates in Wooly Patch, an altered rock encountered at West Spur, Columbia Hills, by the Spirit rover in Gusev crater, Mars, *Journal of Geophysical Research* **111**.

Watkins, J. J., Behr, H. J. and Behr, K. (2011): Fossil microbes in opal from Lightning Ridge – implications for the formation of opal, *Quarterly Notes, Geological Survey of New South Wales* **136**, 1-21.

White, S. N. (2009): Laser Raman spectroscopy as a technique for the identification of seafloor hydrothermal and cold seep minerals, *Chemical Geology* **259**, 240-252.

Wray, R. A. L. (2011): Alunite formation within silica stalactites from the Sydney Region, South-eastern Australia, *International Journal of Speleology* **40**(2), 109-116.